American Mineralogist, Volume 89, pages 1464–1473, 2004

The crystal-structure of synthetic $NaNa_2Mg_5Si_8O_{21}(OH)_3$, a triclinic $C\bar{1}$ amphibole with a triple-cell and excess hydrogen

FERNANDO CÁMARA,[1,*] ROBERTA OBERTI,[1] GIANCARLO DELLA VENTURA,[2] MARK D. WELCH,[3] AND WALTER V. MARESCH[4]

[1]CNR-Istituto di Geoscienze e Georisorse, sezione di Pavia, via Ferrata 1, I-27100 Pavia, Italy
[2]Dipartimento di Scienze Geologiche, Università di Roma Tre, Largo S. Leonardo Murialdo 1, I-00146 Roma, Italy
[3]Department of Mineralogy, The Natural History Museum, Cromwell Road, London SW7 5BD, U.K.
[4]Institut für Geologie, Mineralogie und Geophysik, Ruhr-Universität Bochum, 44780 Bochum, Germany

ABSTRACT

Synthetic $NaNa_2Mg_5Si_8O_{21}(OH)_3$ is the first triclinic member of the amphibole group, and has a tripling of the unit cell in the **b** direction. The space group is $C\bar{1}$ and the triple-*b* repeat gives $Z = 6$. The unit-cell parameters are: $a = 9.883(2)$, $b = 54.082(9)$, and $c = 5.277(1)$ Å, $\alpha = 90.045(4)°$, $\beta = 103.068(3)°$, $\gamma = 89.960(4)°$, and $V = 2748(1)$ Å^3. The crystal structure has been refined to $R_1 = 7.6$ and $wR_2 = 16.7\%$ for the 1835 reflections with $F_o > 4\sigma_F$ and for 4832 supercell reflections in the 2θ range 2–25°, respectively. The structure is pseudo-monoclinic, but both the intensity distribution and refined model indicate space group $C\bar{1}$. Compared with the common *C*2/*m* amphibole structure, the two halves of an I-beam unit are no longer mirror-related, and the overall structure can be rationalized in terms of two different types of I-beam occurring in the unit cell. The first (with multiplicity 2) is centrosymmetric, and the second (with multiplicity 4) is non-centrosymmetric. There are also significant displacements of the cations, especially at the M4 sites, from their corresponding locations in the *C*2/*m* structure. The correlated displacements of Na atoms at the M4 sites permit incorporation of excess protons in pseudo-tetrahedral cavities between two adjacent chains of tetrahedra belonging to different I-beams. Bond-valence calculations and crystal-chemical analysis suggest that excess protons are bonded to O atoms at the O4 sites, and are hydrogen bonded to O atoms at adjacent O2 sites. The infrared spectrum of the amphibole in the principal OH-stretching region has a triplet of sharp bands at 3740, 3727, and 3711 cm^{-1}, which are assigned to the three independent "normal" O3-H groups in the triclinic structure. There is an additional intense and very broad absorption at 3430 cm^{-1} that is resolved only when adsorbed moisture is removed. This band is assigned to the extra H in the structure. All the details provided by structure refinement and the proposed location of the excess H atoms is in accord with previous HRTEM and ^{29}Si- and ^{1}H MAS NMR studies of this amphibole.

INTRODUCTION

Synthetic clinoamphiboles with proton contents exceeding two atoms per formula unit (apfu) were first reported by Gier et al. (1964). The specific synthetic amphibole composition examined here was first described by Witte et al. (1969), who suggested monoclinic symmetry and unit formula $^{A}Na^{B}Na_2{}^{C}Mg_5{}^{T}Si_8O_{21}(OH)_3$. Synthetic amphiboles with "excess protons" have also been synthesized and characterized in several unpublished theses on the Na_2O-MgO-SiO_2-H_2O system at the Universities of Edinburgh and Bochum (e.g., Witte 1975; Welch 1987; Ruthmann 1989). In these studies, the OH content was evaluated in several different ways: (1) from H_2O contents calculated as the difference from 100 wt% by bulk wet chemical analysis; (2) from H_2O contents obtained by weight-loss techniques on experimental products; (3) from H_2O contents obtained by vacuum extraction (followed by either manometric measurements or coulometric titration) from experimental products; (4) from the Na:Mg:Si ratios of the starting material in experiments leading to single-phase amphibole, assuming amphibole stoichiometry; (5) from Na:Mg:Si ratios obtained by bulk wet-chemical analysis of purified synthesis products, assuming amphibole stoichiometry; (6) from the Na:Mg:Si ratios of amphibole products obtained by electron microprobe analysis. The presence of excess protons was corroborated by all these techniques.

In an unsuccessful attempt to localize the excess proton in the amphibole structure by neutron diffraction, Maresch et al. (1991) reported a new synthesis and a more detailed characterization of $^{A}Na^{B}Na_2{}^{C}Mg_5{}^{T}Si_8O_{21}(OH)_3$. On the basis of Rietveld refinement of X-ray powder- and electron-diffraction data, these authors deduced triclinic symmetry with space group *C*1 or $C\bar{1}$, and $\alpha = 89.776(3)$ and $\gamma = 90.27(4)°$, and suggested the existence of a superstructure with a tripled *b* unit-cell edge. Unless extreme care was taken to avoid beam damage, the super-structure reflections usually disappeared after a few seconds of irradiation; however, the perseverance of splitting in diffraction spots in twinned crystals indicated that the structure remained triclinic. Using high-*T* X-ray powder diffraction and differential scanning calorimetry, Maresch et al. (1991) also recognized a reversible triclinic-to-monoclinic phase transition at around 100–160 °C. More recently, Liu et al. (1996) characterized this amphibole

* E-mail: camara@crystal.unipv.it

by combining EMP of some single crystals and water analysis of the bulk product, and showed that it is indeed close to the nominal stoichiometry. They also did a ^{29}Si, ^{23}Na, and ^{1}H MAS NMR study across the phase transition, inferred a tripled superstructure for the triclinic low-*T* polymorph, and showed that the phase transition is related to a shift of the excess protons from a special position in the monoclinic symmetry.

Improvements in both analytical techniques and in the power and sensitivity of X-ray single-crystal diffractometers now allow reliable characterization of very fine-grained synthetic material. A single crystal suitable for X-ray data collection was found in the original experimental powder used by Maresch et al. (1991) and Liu et al. (1996) (code HMR-BO), and characterized by structure refinement. Here, we report the crystal-chemistry and the FTIR analysis of the $^{A}Na^{B}Na_2{}^{C}Mg_5{}^{T}Si_8O_{21}(OH)_3$ compound, and rationalize previous findings in the light of the new data.

Synthesis and characterization of the sample

The $NaNa_2Mg_5Si_8O_{21}(OH)_3$ sample analyzed here was synthesized from a silicate gel according to the methodology of Hamilton and Henderson (1968) using routine hydrothermal techniques in cold-seal pressure vessels (e.g., Vitek and Maresch 1985). As noted above, this is the same product as that examined by Maresch et al. (1991) and Liu et al. (1996), where the results of powder X-ray diffraction, HRTEM, SEM, and EMPA studies are also given. The synthetic product was obtained at 600 °C/1 kbar. These conditions were chosen on the basis of the work of Witte (1975), which indicates a stability field for $NaNa_2Mg_5Si_8O_{21}(OH)_3$ between 560 and 630 °C at 1 kbar in the system Na_2O-MgO-SiO_2-H_2O. The water content of the bulk synthesis product was initially obtained by hydrogen extraction and manometry, giving 2.87 OH per formula unit (pfu). Two further independent determinations based on vacuum heating and coulometric titration yielded 3.09(18) OH pfu. This information, combined with EMP data, gives Na = 2.93(8), Mg = 5.04(5), and Si = 8.00(2) apfu, which corresponds closely to the nominal stoichiometry. Liu et al. (1996) reported the presence of triple-chain-silicate impurities in the form of either discrete crystals or (0*k*0) lamellae, and estimated their concentration to be a few vol% in the synthetic products.

X-ray data collection, structure solution, and refinement

Single crystals suitable for X-ray analysis were hand picked from the powder, consisting of grains generally <10 μm in size. Very few larger crystals were found, up to 10–20 μm in diameter and 100 μm in length. Some crystals had poor diffraction quality, but one crystal 90 × 10 × 8 μm in size had excellent diffraction behavior and was used for the analysis. Data collection was done at CNR-IGG-PV with a Bruker-AXS SMART Apex single-crystal diffractometer working with graphite-monochromatized Mo*K*α X-radiation at 55 kV and 30 mA; the crystal-to-detector distance was 5.0 cm. Three-dimensional data collected in the range 2–30° θ were integrated and corrected for Lorentz, polarization, and background effects using the SAINT+ software version 6.2 (Bruker AXS). Unit-cell dimensions were calculated from least-squares refinement of the positions of all of the collected reflections. A frame width of 0.2° in ω was used to collect 900 frames per batch in three batches at different φ values (0°, 120°, 240°) with 120 s count time per image.

Based upon the results of Maresch et al. (1991), unit-cell parameters were refined unconstrained in triclinic symmetry, giving a = 9.883(2), b = 18.027(9), c = 5.277(1) Å, α = 90.045(4), β = 103.068(3), γ = 89.960(4)°, V = 915.89 Å^3. All the cell edges are smaller than those obtained at room T by XRPD analysis [Maresch et al. (1991): a = 9.9313(5), b = 18.111(1), c = 5.3017(3) Å, α = 89.776(3), β = 103.035(3), γ = 90.271(4)°] and the α and γ angles only deviate slightly from monoclinic symmetry. Reflections with $h + k = 2n + 1$ are absent. Among the 7946 unique reflections, 5177 have indexes at ± 1/3 *k*; 655 reflections in this latter subset have $I > 2\sigma_I$ (the highest I/σ_I being 27). This feature indicates a superstructure based upon a tripled *b* edge, as noticed previously by Maresch et al. (1991) by HRTEM.

Because the shape of the unit cell is close to monoclinic, the data were first treated with the standard *C*2/*m* model for amphiboles (b = 18.027 Å; 1379 unique reflections). Raw intensity data were corrected for absorption based on Laue group 2/*m* using the SADABS v. 2.03 program (Sheldrick 1996), giving R_{merge} = 9.1%. A weighted full-matrix least-squares refinement on F_o^2 (SHELXL-97; Sheldrick 1997a) gave full cation occupancy within the standard deviations. Although the refined parameters were compatible with the crystal size (R_1 = 8.7% for 764 $F_o > 4\sigma_{Fo}$, and wR^2 = 21.7 % for all data; goodness of fit, GooF, = 1.031; 102 variable parameters), the anisotropic displacement parameter (adp) for the M4 site always showed non-positive components.

Structure refinement was also done the in $C\bar{1}$ triclinic symmetry while maintaining the standard unit cell (b = 18.027 Å, 2648 unique observations). Correction for absorption of the raw intensity data gave R_{merge} = 6.3%. The space group $C\bar{1}$ implies doubling the numbers of T and O1, O2, O4, O5, and O6 sites. The anisotropic refinement for all atoms but M4 (which again gave non-positive components of the adp) gave R_1 = 9% for the 1290 $F_o > 4\sigma_F$ and wR^2 = 22.7 % for all data (GooF = 1.036; 187 variable parameters). The refined parameters did not justify use of a triclinic model, and the differences in the individual bond lengths calculated for those sites no longer equivalent in space group $C\bar{1}$ were within the standard deviation.

Integration of all intensity data with the superstructure cell having a triple *b* edge and triclinic symmetry (b = 54.082 Å) followed by correction for absorption gave R_{merge} = 13.9% for the 7946 unique reflections. The superstructure reflections beyond 25° θ are very weak; therefore, the structure was solved in $C\bar{1}$ using a reduced data set (θ-range = 2–25°, 4832 unique reflections, R_{merge} = 10.4%), using direct methods (SHELXS; Sheldrick 1997b), which allowed location of the Si and Mg atoms. The remaining atoms were located on difference-Fourier maps. Twenty-five cation sites (12 Si, 8 Mg, and 5 Na atoms) and 36 anion sites were inserted in the model and refined isotropically, giving R_1 = 9.2% for the 1835 $F_o > 4\sigma_F$ and wR_2 = 24.7 % for all data (GooF = 0.903, 232 variable parameters). A fully anisotropic refinement gave an unstable model with several non-positive-definite adp components for 10 anion sites. The final cycles were done using an anisotropic model for the cations and an isotropic model for the anions (371 variable parameters), giving R_1 = 7.6% for the 1835 $F_o > 4\sigma_F$ and wR_2 = 16.7% (GooF = 0.876). Difference-Fourier maps showed three independent H atoms bonded to the O3 atoms, corresponding to 2 OH groups pfu; these were included in the model, but their coordinates were kept fixed and only their isotropic displacement parameters were refined. The excess protons which would provide the third OH group pfu could not be located from difference-Fourier maps. Refinement results are summarized in Table 1. Final atom coordinates are reported in Table 2. Table 3[1] lists observed and calculated structure factors. The final model shows different geometries for the paired sites which are no longer equivalent in the $C\bar{1}$ space group, which are beyond the estimated standard deviations (Table 4). A sketch of the structure is shown in Figure 1.

The crystal structure of $NaNa_2Mg_5Si_8O_{21}(OH)_3$

A site nomenclature for the new triclinic structure of the amphibole of this work was derived following the scheme used by Hawthorne (1983) for the case of monoclinic and orthorhombic structures. The structure is shown in Figure 1a. The triclinic structure based on a tripled *b* edge can be described in terms of two distinct I-beams:

[1]For a copy of Table 3, Document AM-04-070, contact the Business Office of the Mineralogical Society of America (see inside cover of a recent issue for price information). Deposit items may also be available on the American Mineralogist web site at http://www.minsocam.org.

Table 1. Selected crystal and refinement data

a (Å)	9.883(2)
b (Å)	54.082(9)
c (Å)	5.277(1)
α (°)	90.045(4)
β (°)	103.068(3)
γ (°)	89.960(4)
V (Å^3)	2747.66
Space group	$C\bar{1}$
θ range (°)	2–25
no. F all	4832
no. F obs	1835
R merge (%)	10.4
R_1 $F_o > 4\sigma_{Fo}$(%)	7.6
wR_2 (%)	16.7

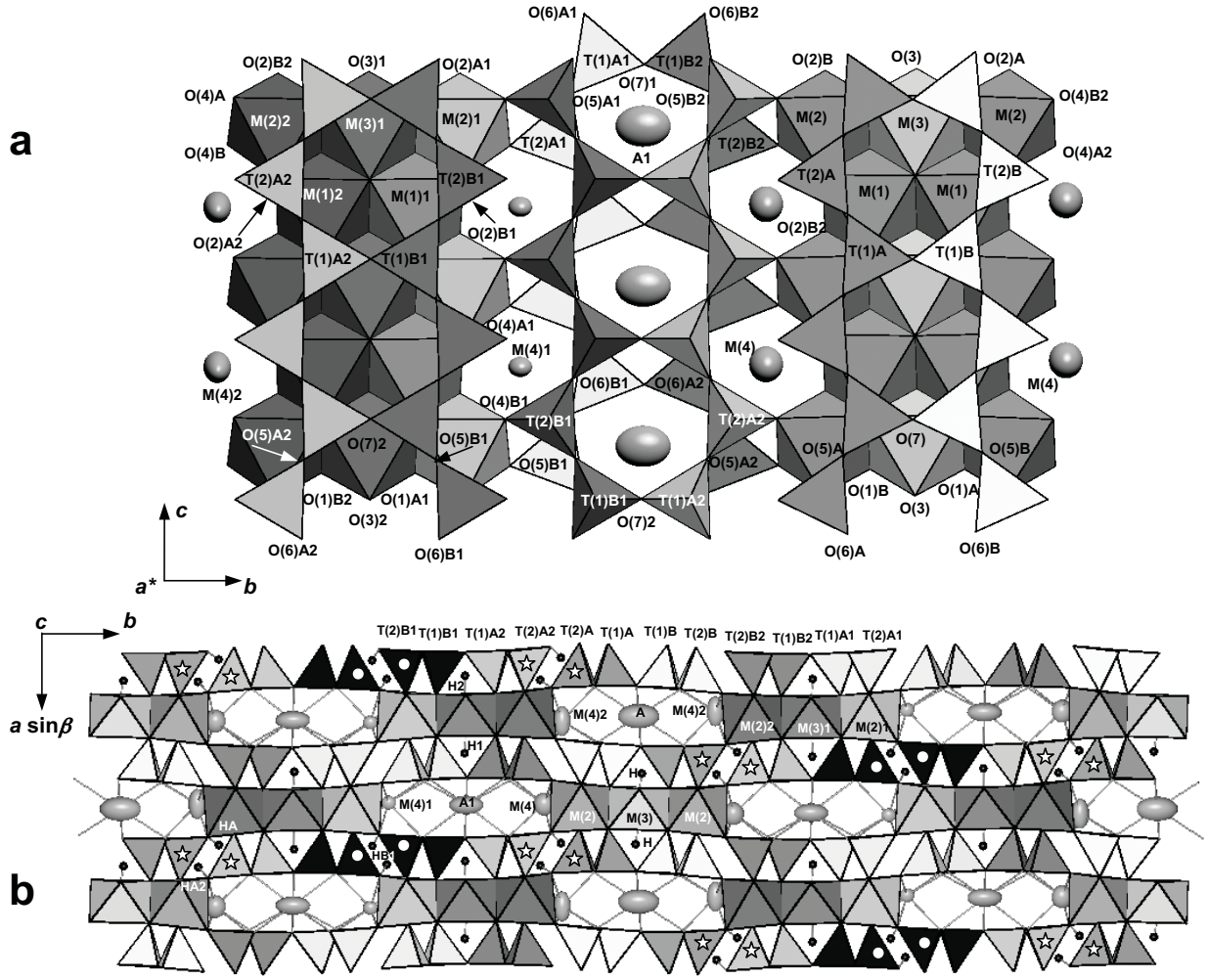

FIGURE 1. Site nomenclature for the triclinic-supercell structure (b = 54.082 Å) of synthetic Na $Na_2Mg_5Si_8O_{21}(OH)_3$; (**a**) projection onto (100); (**b**) projection onto (001) (note the distinct positions of the M4 and A sites). Ellipsoids are drawn at 95% probability. Figure 1b also shows the calculated position for the excess H atoms (HB1, HA, and HA2). Images made using XtalDraw (Downs and Hall-Wallace 2003).

***I-beam I* is centrosymmetric.** The two sides of the double-chain of tetrahedra in the (100) projection are no longer equivalent, and are named A and B in analogy with the *P*2/*a* amphibole structure (Hawthorne 1983): T1A, T2A, T1B, and T2B. These sites repeat themselves (according to $\bar{1}$) in the double chain below the strip of octahedra. *I-beam I* has three 6-coordinated sites (M1, M2, and M3), and one 7-coordinated M4 site. With the exception of O3 and O7, all anion sites are duplicated with respect to the *C*2/*m* structure, and are named with regard to the T sites to which they are bonded, e.g., O1A and O1B. Only one independent H site is present. The nearby Na atom at the A site is 6-coordinated and has point symmetry $\bar{1}$.

***I-beam II* is non-centrosymmetric.** Therefore, the T sites above and below the ribbon of octahedra are no longer equivalent, and a third index must be added to the site name: it is 1 when the tetrahedra are adjacent to *I-beam I*, e.g., T1A1, T2A1, T1B1, and T2B1, and 2 when they are adjacent to *I-beam II*, e.g. T1A2, T2A2, T1B2, and T2B2. *I-beam II* has five independent octahedral sites: M11, M12, M21, M22, and M31, and two independent 7-coordinated M4 sites, M41 and M42, where the labels 1 and 2 have same meaning as for the T sites. *I-beam II* has twenty-four anion sites. With the exceptions of O31, O32, O71, and O72, for which the index 1 or 2 is arbitrarily chosen, O atoms take their designations from the T site to which they are bonded. Two independent H atoms, H1 and H2, are bonded to O31 and O32, respectively. Above and below *I-beam II*, there are 8-coordinated A1 sites with point symmetry 1 (Fig. 1b).

A useful measure of the difference between the two parts of the double-chains of tetrahedra is provided by the O5-O6-O5 angles (Table 4). In *I-beam I*, the double chain is O rotated, and both the A and B chains have O5-O6-O5 angles similar to those found in *C*2/*m* amphiboles (O5A-O6A-O5A = 172.8° and O5B-O6B-O5B = 170.4°; see Hawthorne 1983 for references). In *I-beam II*, one double chain is S-rotated (O5A2-O6A2-O5A2 = 183.9° and O5B1-O6B1-O5B1 = 184.0°), whereas the other double-chain is O-rotated (O5A1-O6A1-O5A1 = 162.4° and O5B2-O6B2-O5B2 = 163.5°).

The $C\bar{1}$ symmetry for the triple-*b* cell derives from the fact that the two distinct I-beams alternate along **b** in the sequence *I-II-II-I-II-II-I*, the two adjacent *I-beams II* being related by a

TABLE 2. Atom coordinates and anisotropic-displacement factors for crystal HMR-BO no. 1

Atom	x/*a*	y/*b*	z/*c*	U_{eq}	U_{11}	U_{22}	U_{33}	U_{12}	U_{13}	U_{23}
T1A	–0.2743 (3)	0.02996 (6)	0.7205 (6)	0.0138 (8)	0.0113 (18)	0.0103 (20)	0.0158 (18)	–0.0027 (14)	–0.0057 (14)	0.0059 (14)
T2A	0.7262 (3)	0.05735 (6)	0.2168 (6)	0.0141 (8)	0.0117 (18)	0.0128 (20)	0.0158 (18)	–0.0038 (14)	–0.0009 (14)	–0.0004 (14)
T1B	0.2840 (3)	0.02651 (6)	0.2948 (6)	0.0124 (8)	0.0091 (18)	0.0091 (19)	0.0144 (18)	0.0013 (14)	–0.0070 (14)	–0.0009 (14)
T2B	0.2984 (3)	0.05545 (6)	0.8031 (6)	0.0125 (8)	0.0088 (17)	0.0106 (19)	0.0145 (17)	–0.0028 (14)	–0.0052 (13)	–0.0018 (14)
T1A1	0.2237 (3)	0.19411 (6)	0.6891 (6)	0.0103 (8)	0.0154 (19)	0.0091 (18)	0.0045 (16)	0.0025 (14)	–0.0018 (14)	–0.0044 (13)
T2A1	0.2123 (3)	0.22275 (6)	0.1829 (6)	0.0114 (8)	0.0167 (19)	0.0099 (19)	0.0038 (16)	0.0031 (14)	–0.0059 (13)	–0.0023 (13)
T1A2	–0.2143 (3)	0.13924 (6)	0.2663 (6)	0.0104 (8)	0.0110 (17)	0.0165 (20)	0.0037 (16)	–0.0012 (14)	0.0015 (13)	0.0054 (13)
T2A2	–0.2025 (3)	0.11051 (6)	0.7792 (6)	0.0123 (8)	0.0155 (19)	0.0127 (19)	0.0079 (17)	0.0018 (15)	0.0011 (14)	0.0047 (14)
T1B1	0.7816 (3)	0.19566 (6)	0.2634 (6)	0.0098 (8)	0.0148 (19)	0.0127 (19)	0.0014 (15)	0.0009 (14)	0.0007 (13)	0.0024 (13)
T2B1	0.7146 (4)	0.27655 (6)	0.2307 (6)	0.0153 (8)	0.0286 (21)	0.0083 (19)	0.0082 (17)	–0.0006 (15)	0.0027 (15)	0.0000 (13)
T1B2	0.2290 (3)	0.13774 (6)	0.6939 (6)	0.0106 (8)	0.0082 (17)	0.0132 (20)	0.0095 (17)	0.0015 (14)	0.0003 (13)	–0.0023 (14)
T2B2	0.2236 (3)	0.10980 (6)	0.1892 (6)	0.0103 (8)	0.0083 (17)	0.0156 (20)	0.0082 (17)	–0.0039 (14)	0.0046 (13)	–0.0011 (13)
M1	0.0069 (4)	0.02984 (8)	0.5070 (8)	0.0181 (11)	0.0142 (23)	0.0160 (25)	0.0204 (25)	–0.0001 (19)	–0.0037 (19)	0.0003 (19)
M2	0.0121 (4)	0.06009 (8)	0.0054 (8)	0.0178 (10)	0.0157 (23)	0.0136 (24)	0.0234 (25)	0.0041 (18)	0.0030 (19)	0.0024 (19)
M3	0	0	0	0.0136 (14)	0.0150 (32)	0.0139 (35)	0.0067 (30)	0.0078 (26)	–0.0083 (24)	0.0004 (25)
M11	0.5014 (4)	0.19646 (7)	0.4748 (7)	0.0101 (9)	0.0139 (22)	0.0119 (23)	0.0024 (19)	0.0037 (18)	–0.0027 (16)	–0.0012 (16)
M12	0.5082 (4)	0.13723 (7)	0.4792 (7)	0.0115 (9)	0.0150 (22)	0.0128 (23)	0.0070 (20)	–0.0002 (18)	0.0031 (17)	0.0001 (17)
M21	0.4926 (4)	0.22672 (7)	–0.0320 (7)	0.0113 (9)	0.0111 (21)	0.0158 (24)	0.0044 (20)	–0.0027 (17)	–0.0039 (16)	0.0036 (16)
M22	0.5028 (4)	0.10656 (8)	–0.0313 (8)	0.0157 (10)	0.0172 (23)	0.0163 (24)	0.0154 (22)	–0.0015 (18)	0.0080 (18)	–0.0035 (18)
M31	–0.4945 (4)	0.16667 (8)	–0.0216 (7)	0.0090 (8)	0.0118 (19)	0.0111 (20)	0.0029 (19)	–0.0044 (15)	–0.0007 (15)	0.0007 (15)
M4	0.0263 (6)	0.09136 (11)	0.5241 (11)	0.0402 (15)	0.0462 (37)	0.0400 (37)	0.0403 (36)	–0.0094 (30)	0.0220 (29)	–0.0150 (28)
M41	0.4663 (5)	0.25874 (9)	0.4552 (8)	0.0176 (11)	0.0170 (25)	0.0198 (27)	0.0125 (24)	0.0007 (20)	–0.0039 (19)	0.0010 (19)
M42	0.4738 (6)	0.07400 (10)	0.4547 (10)	0.0412 (16)	0.0787 (45)	0.0265 (34)	0.0288 (31)	0.0169 (31)	0.0338 (31)	0.0123 (25)
A	1/2	0	0	0.0869 (39)	0.0510 (64)	0.1497 (118)	0.0712 (73)	0.0226 (68)	0.0376 (56)	–0.0094 (71)
A1	0.0214 (6)	0.16632 (15)	1.0347 (13)	0.0613 (20)	0.0293 (36)	0.1061 (57)	0.0547 (41)	–0.0126 (36)	0.0224 (31)	0.0017 (37)

O1A	–0.1090 (8)	0.02960 (15)	0.7872 (15)	0.0201 (20)		x/*a*	y/*b*	z/*c*	U_{eq}
O1B	0.1181 (7)	0.02805 (14)	0.2164 (14)	0.0121 (18)	O4B2	0.1533 (8)	0.08374 (14)	0.2094 (14)	0.0155 (19)
O1A1	0.3905 (7)	0.19478 (14)	0.7611 (14)	0.0126 (18)	O5A	0.6617 (8)	0.04459 (15)	0.9383 (15)	0.0258 (21)
O1A2	–0.3788 (7)	0.13801 (13)	0.1910 (14)	0.0095 (18)	O5B	0.3562 (8)	0.04030 (15)	0.0887 (15)	0.0247 (21)
O1B1	0.6155 (7)	0.19553 (14)	0.1905 (14)	0.0124 (18)	O5A1	0.3458 (7)	0.29010 (13)	0.1121 (13)	0.0081 (16)
O1B2	0.3936 (7)	0.13737 (14)	0.7613 (14)	0.0125 (18)	O5A2	–0.1463 (7)	0.12711 (12)	0.0404 (12)	0.0067 (16)
O2A	–0.1080 (8)	0.05698 (14)	0.2829 (15)	0.0179 (20)	O5B1	–0.1526 (7)	0.20763 (13)	1.0352 (13)	0.0142 (18)
O2B	0.1305 (8)	0.05525 (14)	0.7345 (15)	0.0163 (19)	O5B2	0.1610 (7)	0.12182 (13)	0.8972 (13)	0.0086 (16)
O2A1	0.3795 (7)	0.22200 (14)	0.2510 (14)	0.0111 (18)	O6A	0.6649 (8)	0.04161 (15)	0.4330 (15)	0.0236 (20)
O2A2	0.6300 (8)	0.10991 (15)	0.6982 (15)	0.0206 (21)	O6B	0.3485 (8)	0.03643 (15)	0.5894 (15)	0.0237 (20)
O2B1	0.6184 (8)	0.22413 (14)	0.6972 (14)	0.0139 (18)	O6A1	0.1616 (7)	0.20230 (13)	0.3912 (13)	0.0087 (16)
O2B2	0.3905 (7)	0.11108 (13)	0.2544 (13)	0.0101 (18)	O6A2	–0.1508 (8)	0.12565 (15)	0.5402 (15)	0.0211 (19)
O3	0.8951 (9)	0.00054 (15)	0.2896 (16)	0.0169 (21)	O6B1	0.6545 (7)	0.29069 (13)	0.4615 (13)	0.0120 (17)
O31	0.4012 (8)	0.16650 (14)	0.2711 (14)	0.0138 (19)	O6B2	0.1669 (7)	0.12881 (14)	0.3937 (14)	0.0171 (18)
O32	0.6131 (8)	0.16695 (14)	0.6867 (15)	0.0149 (19)	O7	0.3388 (7)	–0.00203 (14)	0.2863 (14)	0.0130 (18)
O4A	0.6528 (7)	0.08412 (13)	0.2152 (14)	0.0114 (18)	O71	0.1672 (8)	0.16558 (14)	0.7118 (14)	0.0166 (19)
O4B	0.3777 (8)	0.08035 (14)	0.8034 (15)	0.0164 (19)	O72	–0.1550 (8)	0.16755 (15)	0.2891 (15)	0.0209 (20)
O4A1	0.3607 (8)	0.25233 (15)	–0.2083 (15)	0.0237 (21)	H	0.8088	0.00306	0.2645	0.0000 (254)
O4A2	–0.1258 (8)	0.08489 (15)	–0.2022 (16)	0.0209 (20)	H1	0.3002	0.16791	0.2525	0.0447 (397)
O4B1	0.6389 (8)	0.24954 (15)	0.2020 (15)	0.0222 (21)	H2	0.7182	0.16750	0.7383	0.0287 (340)

center of symmetry at the A site (Fig. 1b).

Na atoms at the M41 and M42 sites are displaced significantly along the **a** and **c** axes relative to the analogous positions on the diad in the *C*2/*m* structure. Their coordination reduces from 8 in *C*2/*m* to 7 in $C\bar{1}$, one O5 anion always being more than 3 Å away in the latter structure. Around the M41 and M42 sites, there is one short and one long M4-O4 distance, as well one short and one long M4-O2 distance. A similar pattern also occurs at the adjacent M21 and M22 sites. These unusual displacements of the M4 and M2 cations underpin the discussion that follows on the possible location of the third proton in the formula unit.

Fourier-Transform infrared spectroscopy

FTIR data were collected in transmission mode from powdered material embedded in KBr, using a Nicolet Magna 760 spectrophotometer equipped with a KBr beamsplitter and a DTGS detector; 64 scans were averaged for each spectrum. The room-*T* spectrum in the OH-stretching region (Fig. 2a) has three distinct bands at 3740, 3727, and 3711 cm^{-1} which are assigned to the O3 hydroxyl groups of the $C\bar{1}$ amphibole structure. This spectrum is almost identical to that given by Maresch and Langer (1976). In addition, the room-*T* spectrum shows a very broad absorption at lower frequencies, in the 3600–2600 cm^{-1} region (Fig. 2b, top). Molecular H_2O (moisture) adsorbed on the sample and KBr pellet is well known to absorb at around 3200 cm^{-1}. However, upon closer inspection, the broad absorption in the 3600–2600 cm^{-1} range is seen to be composed of at least two overlapping bands, the first at 3200 cm^{-1} and the second around 3400 cm^{-1} (Fig. 2b, top). To remove adsorbed moisture and resolve these components, a second spectrum was collected at 250 °C using a SPECAC micro-furnace placed inside the spectrophotometer. The 250 °C spectrum (Fig. 2b, middle) shows that a very broad and intense band occurs at 3430 cm^{-1}. The intensity of this band does not decrease, even with prolonged heating (>24 h). Therefore, we assign this band to structural hydroxyl groups involved in significant hydrogen bonding. Loss of adsorbed moisture with increasing *T* is completely reversible, as indicated by the spectral changes in the principal OH-stretching region: the spectrum collected immediately after the temperature drop to room *T* (Fig. 2b, bottom) is identical to the one collected before annealing. Note that the band triplet due to "normal" OH groups (Fig. 2a) at 250 °C merges into a single band (Fig. 2b) as a consequence of the reversible triclinic ↔ monoclinic

TABLE 4. Selected bond-lengths (Å) and angles (°) for crystal HMR-BO n. 1

T1A	-O1A	1.592	(8)	T1B	-O1B	1.599	(8)	T1A2	-O1A2	1.586	(8)	T1B1	-O1B1	1.598	(8)	T1A1	-O1A1	1.606	(8)
	-O5A	1.635	(9)		-O5B	1.613	(9)		-O5A2	1.632	(7)		-O5B1	1.628	(8)		-O5A1	1.621	(7)
	-O6A	1.628	(8)		-O6B	1.632	(8)		-O6A2	1.617	(8)		-O6B1	1.623	(7)		-O6A1	1.615	(7)
	-O7	1.637	(8)		-O7	1.640	(8)		-O72	1.634	(9)		-O72	1.638	(9)		-O71	1.655	(8)
<T1A-O>		1.623		<T1B-O>		1.621		<T1A2-O>		1.617		<T1B1-O>		1.622		<T1A1-O>		1.624	
V (Å³)		2.19		*V* (Å³)		2.17		*V* (Å³)		2.16		*V* (Å³)		2.18		*V* (Å³)		2.19	
TAV		11.09		TAV		17.33		TAV		12.81		TAV		15.90		TAV	13.70	TAV	

T1B1	-O1B1	1.598	(8)	T1A1	-O1A1	1.606	(8)	T1B2	-O1B2	1.584	(8)	T2A	-O2A	1.597	(8)	T2B	-O2B	1.617	(8)
	-O5B1	1.628	(8)		-O5A1	1.621	(7)		-O5B2	1.635	(7)		-O4A	1.618	(8)		-O4B	1.559	(8)
	-O6B1	1.623	(7)		-O6A1	1.615	(7)		-O6B2	1.637	(8)		-O5A	1.618	(9)		-O5B	1.697	(8)
	-O72	1.638	(9)		-O71	1.655	(8)		-O71	1.635	(8)		-O6A	1.646	(9)		-O6B	1.681	(9)
<T1B1-O>		1.622		<T1A1-O>		1.624		<T1B2-O>		1.623		<T2A-O>		1.620		<T2B-O>		1.638	
V (Å³)		2.18		*V* (Å³)		2.19		*V* (Å³)		2.18		*V* (Å³)		2.16		*V* (Å³)		2.23	
TAV		15.90		TAV		13.70	TAV		16.20			TAV		22.73		TAV		34.71	

T2A1	-O2A1	1.611	(8)	T2B2	-O2B2	1.609	(7)	M1	-O1A	2.065	(9)	M11	-O1A1	2.060	(8)	M12	-O1A2	2.081	(8)
	-O4A1	1.548	(9)		-O4B2	1.586	(8)		-O1B	2.081	(8)		-O1B1	2.072	(8)		-O1B2	2.065	(8)
	-O5A1	1.682	(7)		-O5B2	1.658	(7)		-O2A	2.058	(9)		-O2A1	2.028	(8)		-O2A2	2.083	(9)
	-O6A1	1.713	(7)		-O6B2	1.676	(8)		-O2B	2.039	(9)		-O2B1	2.083	(9)		-O2B2	2.034	(8)
<T2A1-O>		1.639		<T2B2-O>		1.632			-O3	2.115	(9)		-O31	2.069	(9)		-O31	2.075	(9)
V (Å³)		2.24		*V* (Å³)		2.22			-O3	2.078	(9)		-O32	2.112	(9)		-O32	2.084	(9)
TAV		27.27		TAV		21.24		<M1-O>		2.073		<M11-O>		2.070		<M12-O>		2.070	
								V (Å³)		11.68		*V* (Å³) 1		11.65		*V* (Å³)		11.67	
								OAV		36.92		OAV		35.09		OAV		31.13	

M3	-O1A	2.106	(8)	M4	-O2A	2.465	(10)	M42	-O2A2	2.629	(10)	M2	-O1A	2.203	(9)	M21	-O1A1	2.167	(8)
	-O1A	2.106	(8)		-O2B	2.364	(10)		-O2B2	2.329	(9)		-O1B	2.194	(9)		-O1B1	2.248	(9)
	-O1B	2.089	(7)		-O4A2	2.335	(9)		-O4A	2.458	(9)		-O2A	2.090	(9)		-O2A1	2.074	(8)
	-O1B	2.089	(7)		-O4B2	2.333	(9)		-O4B	2.279	(9)		-O2B	2.058	(9)		-O2B1	2.100	(8)
	-O3	2.031	(8)		-O5B2	2.679	(9)		-O5B	2.718	(10)		-O4A2	2.045	(9)		-O4A1	1.984	(9)
	-O3	2.031	(8)		-O6A2	2.564	(10)		-O6A	2.597	(10)		-O4B2	2.016	(9)		-O4B1	2.081	(9)
<M3-O>		2.076			-O6B2	2.635	(9)		-O6B	2.563	(10)	<M2-O>		2.101		<M21-O>		2.109	
V (Å³)		11.71		<M4-O>		2.482		<M42-O>		2.510		*V* (Å³)		12.16		*V* (Å³)		12.26	
OAV		39.34										OAV		39.04		OAV		47.29	

M22	-O1A2	2.240	(9)	M31	-O1A1	2.081	(9)	M41	-O2A1	2.330	(9)	A1	-O5A1	2.889	(10)				
	-O1B2	2.146	(9)		-O1A2	2.095	(8)		-O2B1	2.554	(9)		-O5A2	2.696	(10)				
	-O2A2	2.112	(9)		-O1B1	2.079	(9)		-O4A1	2.281	(9)		-O5B1	2.819	(10)				
	-O2B2	2.079	(8)		-O1B2	2.115	(8)		-O4B1	2.444	(9)		-O5B2	2.944	(10)				
	-O4A	2.119	(8)		-O31	2.042	(8)		-O5A1	2.569	(8)		-O6A1	2.840	(10)				
	-O4B	1.953	(9)		-O32	2.060	(8)		-O6A1	2.674	(8)		-O6B2	2.923	(10)				
<M22-O>		2.108		<M31-O>		2.078			-O6B1	2.534	(8)		-O71	2.469	(9)				
V (Å³)		12.25		*V* (Å³)		11.75		<M41-O>		2.484			-O72	2.430	(10)				
OAV		46.48		OAV		39.84						<A1-O>		2.751					

								A	-O5B ×2	2.699	(8)								
									-O5A ×2	2.953	(8)	H	-O3	0.843					
O5A2-O6A2-O5A2	183.9	(5)	O5A-O6A-O5A	172.9	(5)	O5A1-O6A1-O5A1	162.0	(5)		-O7 ×2	2.434	(7)	H1	-O31	0.983					
O5B1-O6B1-O5B1	184.0	(5)	O5B-O6B-O5B	170.4	(5)	O5B2-O6B2-O5B2	163.5	(5)	<A-O>		2.695		H2	-O32	1.013					

Note: The coordination radius is 3 Å for the M4 and the A sites.

phase transition which occurs around 100–160 °C in this amphibole (Maresch et al. 1991; Liu et al. 1996). The behavior at the transition will be discussed in a forthcoming paper.

The location of excess H

The possibility of OH contents beyond the stoichiometric value of 2.0 apfu in amphiboles has been debated since Phillips (1963) first suggested that H in excess of 2.0 apfu may be present in amphiboles and may be located at random but diametrically opposed positions within the A-cavity. Leake (1968) noted that some of the 431 "superior" analyses available for amphiboles in the calcium-sodium group had OH + F + Cl between 2.00 and 2.99 apfu. Kemp and Leake (1975) reported analyses of two hornblendes enriched in H (2.60 apfu). They concluded that, wherever located (either as H_3O^+ at the A site or as OH at some of the basal O atoms of the double-chain of tetrahedra), the excess H balances the observed substitution of large amounts of Al after Si.

The recent availability of ion-microprobe procedures for in situ quantification of H has allowed easier and more accurate determination of the H content in natural amphiboles. Although most of these analyses have been done on mantle amphiboles with at least partial dehydrogenation (e.g., Zanetti et al. 1997; King et al. 1999), many analyses were done on crustal amphiboles (e.g., Hawthorne et al. 1998, 2001; Oberti et al. 2003) but none supported the presence of excess protons [even in the case of some good candidates from the Leake (1968) compilation; CNR-IGG-PV, unpublished].

In contrast, several experimental studies have led to synthetic amphiboles with persuasive evidence for excess H beyond 2.0 apfu, even though the actual location within the crystal structure has remained a matter of debate. Numerous studies of amphiboles in the system Na_2O-MgO-SiO_2-H_2O have provided strong compositional evidence for excess H (Gier et al. 1964; Witte et al. 1969; Welch et al. 1992). Further examples of systems containing amphiboles with excess H are Li_2O-MgO-SiO_2-H_2O (Maresch and Langer 1976), Li_2O-Na_2O-MgO-SiO_2-H_2O (Oberti et al. 2000), the hastingsitic amphiboles reported by Semet (1973), and the richterite(50)-tremolite(50) solid solutions reported by Kuroda et al. (1975). Semet (1973) characterized by Mössbauer and IR spectroscopy a series of magnesiohastingsites synthesized at different f_{O_2} conditions, and observed significant reduction in $^{M2}Fe^{3+}$ at low f_{O_2}, which was accompanied by the growth of a broad absorption band, centered below 3640 cm^{-1} in the infrared OH-stretching region. His conclusion was that excess H (possibly occurring at the O4 sites, the most underbonded site in the amphibole structure) could balance Fe reduction. Kuroda et al. (1975) reported bulk water contents determined by hydrogen extraction in excess of 3 wt%, but did not speculate on the crystal-chemical significance of their results.

Liu et al. (1996) studied the triclinic-to-monoclinic transition in $NaNa_2Mg_5Si_8O_{21}(OH)_3$ by ^{29}Si, ^{23}Na, and ^{1}H MAS NMR spectroscopy and proposed that the excess protons are shared by two adjacent O4 atoms and point in between two equivalent T2 tetrahedra facing base to base. It was suggested that during the transition, these protons progressively order on the diad axis present in the monoclinic *C*2/*m* space group.

Refinement of the crystal structure of $NaNa_2Mg_5Si_8O_{21}(OH)_3$ provides a more suitable location and also a crystal-chemical mechanism that allows incorporation of excess protons. This

discussion can be followed with the help of Figures 1b and 3. The main difference between the structure of HMN-BO n. 1 and that of normal amphiboles with 2 OH pfu is the off-centering of the M4 sites from a line corresponding to the diad of *C*2/*m* amphiboles. The Na atoms at the M4 sites also have anomalous adp values, which indicates unusual static disorder. In all other known amphibole space groups, the largest component of the adp is along the **b** axis and represents static ordering of cations of different sizes substituting at this site (Mg, Fe, and Li vs. Na and Ca). Here, we have only one cation, Na, and the observed behavior is the key to understanding the location of excess H. In the *I-beam II* modules, pairs of adjacent M41 sites have two different and alternating spatial relations along **a** *sin* β, one with a shorter M41-M41 separation (4.508 Å) and the other with a longer separation (5.599 Å). In the latter case, the two long M41-O4B1 bond-lengths should increase the need for an extra bond-strength contribution at the O4B1 sites, and an excess proton could be hosted in the pseudo-tetrahedral cavity between two T2B1 tetrahedra (black and marked with a white dot in Fig. 1b).

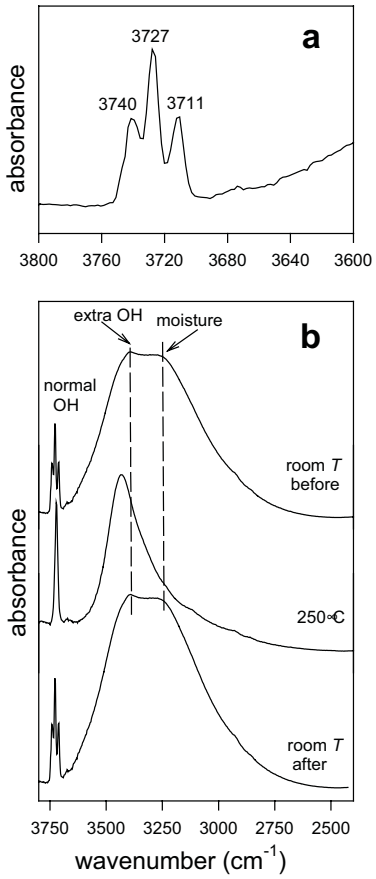

FIGURE 2. FTIR spectra in the OH-stretching region for synthetic $NaNa_2Mg_5Si_8O_{21}(OH)_3$, sample HMR-BO. (**a**) principal OH-stretching region; (**b**) comparison of the entire 3800–2400 cm^{-1} region for the room-*T* sample (top), the 250 °C sample (middle), and the room-*T* sample immediately after the temperature drop (bottom).

A different situation is encountered where M4 sites adjacent to an *I-beam I* (M4) and to an *I-beam II* (M42) alternate along **a** *sin* β. M42 has large adp values, with the major component along **a** *sin* β. It is thus possible to have a proton bonded to the O4A site where Na at the M42 site is displaced away from the pseudo-tetrahedral cavity. Thus, the proton could protrude into the pseudo-tetrahedral cavity between two T2A and T2A2 tetrahedra (medium gray and light gray, both marked with a white star in Fig. 1b).

Using the positional data for a synthetic *C*2/*m* fluororichterite refined by Cameron and Gibbs (1971), Liu et al. (1996) calculated a bond valence incident at the O4 site of 1.6 v.u.. They proposed that excess H may be shared by two O4 atoms, and occupy an average, dynamically disordered position on the diad in the monoclinic phase, but are displaced toward one side of the cavity in the triclinic phase.

We have calculated the bond valences incident at the O4 and O2 sites for the triclinic structure with the triple *b* configuration using the curves of Brown and Altermatt (1985) for Mg-O and Na-O bonds and those of Brese and O'Keeffe (1991) for Si-O bonds. The results are reported in Table 5. There are two pairs of O4 anions sites which are strongly bond-valence deficient (O4A, O4B1 with 1.50 v.u., and O4A2, O4B2 with 1.77 v.u.), and one pair with a nearly ideal value (O4B and O4A1 with 1.96 v.u.). Three O2 sites are also slightly deficient (O2A, O2A2, and O2B1).

As the difference Fourier maps did not provide any experimental evidence, excess protons were located by a trial-and-error process using the following constraints: (1) correct distance to the bond-valence deficient anions; (2) correct geometry for a hydrogen bond of the type O4B1 (donor)-H···O2B1 (acceptor); (3) maximization of cation-H distances. Table 6 lists possible coordinates and interaction distances for excess protons protruding (1) outside and (2) inside the M4 cavity. The local environments of the excess H are sketched in Figure 3. Model 1 (proton outside the M4 cavity) is represented by a gray dot, and model 2 (proton within the M4 cavity) is represented by a white dot. Whereas much longer H···H separations occur with model 2 (see Table 6), there are several very short M4-H distances (1.44, 1.61, and 1.64 Å). Model 1 is thus the preferred choice for the positions of excess H atoms. As this model has very short H···H distances (HA···HA2 = 1.6 and HB1···HB1 = 1.8 Å, respectively), only one

TABLE 5. Calculated bond valences (Brown and Altermatt 1985) incident at the O4 and O2 sites in crystal HMR-BO no. 1

O4A-	T2A	1.016	O4B-	T2B	1.194	O4A1-T2A1	1.228	O4A2-	T2A2	1.152	O4B1-	T2B1	0.976	O4B2-	T2B2	1.108
	M22	0.317		M22	0.496	M21	0.456		M2	0.386		M21	0.351		M2	0.418
	M42	0.170		M42	0.276	M41	0.275		M4	0.237		M41	0.177		M4	0.239
Σ b.v.		1.503			1.966		1.959			1.776			1.504			1.765
O2A-	T2A	1.076	O2B-	T2B	1.020	O2A1-T2A1	1.037	O2A2-	T2A2	1.027	O2B1-	T2B1	1.043	O2B2-	T2B2	1.043
	M1	0.373		M1	0.393	M11	0.405		M12	0.349		M11	0.348		M12	0.398
	M2	0.342		M2	0.373	M21	0.358		M22	0.322		M21	0.333		M22	0.352
	M4	0.167		M4	0.219	M41	0.241		M42	0.107		M41	0.131		M42	0.241
Σ b.v.		1.958			2.005		2.040			1.806			1.856			2.035

TABLE 6. Calculated fractional coordinates and bond-lengths (Å) for the excess H atoms in crystal HMR-BO n. 1

	Option 1			Option 2		
	x/*a*	y/*b*	z/*c*	x/*a*	y/*b*	z/*c*
HB1	0.700	0.243	0.380	0.570	0.243	0.315
HA	0.695	0.095	0.390	0.610	0.084	0.370
HA2	0.815	0.075	0.610	0.907	0.084	0.620
HB1-O2B1		2.260			2.215	
HB1-O4B1		1.056			1.060	
HB1-T2B1		1.997			2.411	
HB1-M41		2.574			1.635	
HB1-M21		2.772			2.020	
HA-O2A2		2.044			2.201	
HA-O4A		1.094			0.999	
HA-T2A		2.281			2.111	
HA-M42		2.555			1.609	
HA-M2		2.652			2.467	
HA2-O2A		2.258			2.280	
HA2-O4A2		1.161			1.061	
HA2-T2A2		2.142			2.084	
HA2-M4		2.405			1.440	
HA2-M2		2.639			2.436	

of the two H positions in a cavity is occupied. With only one of the pair of H sites occupied in each cavity, the atom multiplicities for HB1, HA, and H2A are all 2, leading to one excess H pfu (Z = 6). Each proton would supply 0.4 v.u. to the O4 donor and 0.1 v.u. to the O2 acceptor, in good agreement with the calculations reported in Table 5.

The proposed model for excess protons is supported by the unusual Na positions at M4 sites of this particular amphibole structure, and also by bond-valence calculations. However, the model should be tested by other techniques, such as neutron powder diffraction on deuterated samples, which might allow direct location of the excess protons.

RE-EXAMINATION OF THE AVAILABLE DATA ON SYNTHETIC AMPHIBOLES IN THE SYSTEM Na_2O-MgO-SiO_2-H_2O

Infrared spectra

Maresch and Langer (1976) reported IR spectra in the OH-stretching region for synthetic $Na(NaMg)Mg_5Si_8O_{22}(OH)_2$ and $NaNa_2Mg_5Si_8O_{21}(OH)_3$ amphibole compositions crystallized by Witte et al. (1969). On the basis of the fact that the first sample has two bands (at 3739 and 3716 cm^{-1}) and the second has three bands (at 3740, 3727, and 3711 cm^{-1}) in the principal OH-stretching region, these authors concluded that the band at 3727 cm^{-1} could be assigned to extra protons bonded to the O4 atom. Recently, Iezzi et al. (2004) showed that synthetic $Na(NaMg)Mg_5Si_8O_{22}(OH)_2$ has $P2_1/m$ symmetry, which implies the presence of two independent OH atoms per formula unit and thus of two distinct bands in the IR spectrum. The IR spectra recorded by Maresch and Langer (1976) from the sample synthesized by Witte et al. (1969) can now be interpreted on the basis of a further lowering of symmetry to $C\bar{1}$, as discussed below.

The triplet of sharp bands at 3740–3711 cm^{-1} is assigned to O3H-dipoles directly bonded to three Mg cations facing a filled A-site, i.e., the MgMgMg-^{A}Na-OH configuration (Rowbotham and Farmer 1973; Maresch and Langer 1976; Hawthorne et al. 1997). Richterite, $Na(NaCa)Mg_5Si_8O_{22}(OH)_2$, shows a single absorption band at 3725 cm^{-1} which is assigned to the MgMgMg-^{A}Na-OH local configuration in the structure (Robert et al. 1989; Della Ventura 1992). However, richterite has $C2/m$ symmetry (and only one independent H atom), whereas the sample of this work has $C\bar{1}$ symmetry, and three independent H atoms bonded to O3 anions. The correct estimate of the position of the H atoms is difficult by X-ray techniques, especially when the crystal is small and many reflections are very weak. Nevertheless, the structure refinement gave three different geometrical environments for the three symmetry-independent H atoms. Considering the relative lengths of the three hydroxyl bonds, the 3740 cm^{-1} band is assigned to the shorter O3-H dipole (0.843 Å), the 3727 cm^{-1} band to medium O31-H1 dipole (0.983 Å), and the 3711 cm^{-1} band to the longer O32-H1 dipole (1.013 Å).

On the basis of its behavior during thermal treatment of the sample, the broad 3430 cm^{-1} band can be assigned to excess H in the structure. Both the frequency and the width of this band are compatible with a significant hydrogen-bonded interaction of the proton with the next-nearest-neighbor O atoms. Increasing hydrogen-bond strength is known to negatively shift the hydroxyl stretching frequency and to enhance the bandwidth (Huggins and Pimentel 1956; Nakamoto et al. 1955; Beran and Libowitzky

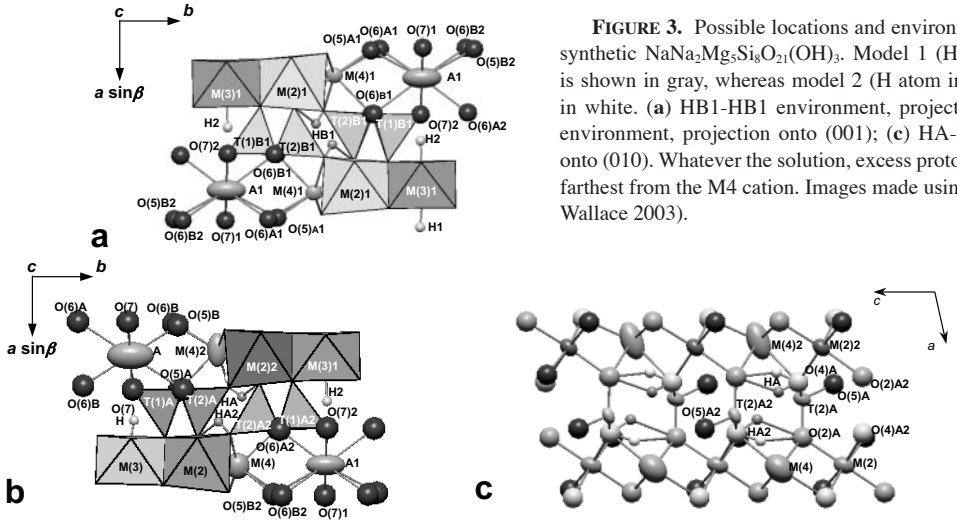

FIGURE 3. Possible locations and environments of the excess protons in synthetic $NaNa_2Mg_5Si_8O_{21}(OH)_3$. Model 1 (H atom outside the M4 cavity) is shown in gray, whereas model 2 (H atom inside the M4 cavity) is shown in white. (**a**) HB1-HB1 environment, projection onto (001); (**b**) HA-HA2 environment, projection onto (001); (**c**) HA-HA2 environment, projection onto (010). Whatever the solution, excess protons are bonded to the O4 atoms farthest from the M4 cation. Images made using XtalDraw (Downs and Hall-Wallace 2003).

1999). In fact, the bandwidth is related to a variety of orientations and may be associated with bent O-H···O configurations (Huggins and Pimentel 1956). The frequency shift is related to the O-H···O distance (Nakamoto et al. 1955, Novak 1974); using these relations, d(O···O) ~2.85 Å is estimated for the O atoms bonded to the extra protons in synthetic Na Na_2 Mg_5 Si_8 O_{21} $(OH)_3$. The d(O···O) distances obtained by structure refinement are as follows: O4A····O2A2 = 2.96, O4A2····O2A = 3.15, and O4B1····O2B1 = 3.00 Å.

MAS NMR spectroscopy

Liu et al. (1996) studied the triclinic-to-monoclinic phase transition of $NaNa_2Mg_5Si_8O_{21}(OH)_3$ by ^{29}Si, ^{23}Na, and ^{1}H MAS NMR and ^{29}Si-^{1}H cross-polarization MAS NMR (CP MAS NMR). Nine different ^{29}Si sites were resolved in the spectrum (Fig. 4), with a further two possible flanking peaks (* in Fig. 4). This result is consistent with twelve independent Si sites in the $C\bar{1}$ cell with a tripled b edge. ^{29}Si-^{1}H CP MAS NMR provides a very effective relaxation mechanism (magnetization transfer) and well-resolved spectra can be obtained in relatively short times. However, unlike normal MAS NMR spectra, the relative intensities of peaks in CP MAS NMR spectra give only semi-quantitative site-populations because peak intensity depends upon how quickly different Si nuclei relax relative to the pulse interval used (i.e., relaxation rates depend upon the Si-H distances involved). The value of the CP MAS NMR experiment is that it gives a more reliable indication of the *number* of different Si sites present in the amphibole.

Welch et al. (1998) examined a series of synthetic $C2/m$ calcic and sodic-calcic amphiboles by ^{29}Si MAS NMR spectroscopy, and found that different cations at the M4 site shift the signals of the Q^2 environments (the T2 sites), whereas the presence and off-centering of the A-site cations along m (not along the diad) may split the Q^3 environments (the T1 sites). Such splitting is not observed in the 240 °C spectrum of monoclinic $NaNa_2Mg_5Si_8O_{21}(OH)_3$ reported by Liu et al. (1996), and so is compatible with the presence of Na at the A2 or the A2/m site. The ^{29}Si CP MAS NMR spectrum at 240 °C (Liu et al. 1996) consists of two very narrow unsplit symmetric peaks due to Si at the T1 and T2 sites. Such a spectrum is compatible only with $C2/m$ symmetry.

The interpretation of the room-T spectrum of the triclinic polymorph is more difficult. As all T1 tetrahedra have similar bond lengths and angles (as do all T2 tetrahedra; Table 4), the spread of chemical shifts (Fig. 4) should be interpreted by considering next-nearest-neighbor cations (other than Si). In the light of the structure determination reported here, the NMR study of Welch et al. (1998), in which correlations between Si chemical shifts and occupancies of the M4 and A sites were recognized, provides a means of tentatively assigning the different Si peaks in Figure 4. Welch et al. (1998) observed a significant effect of the M4 and A cations on the Si chemical shifts; therefore, we focus on the structural variations around Na at the M4 and A sites as the most probable cause of the multiple Q^2 and Q^3 peaks in the room-T spectrum of Na Na_2 Mg_5 Si_8 O_{21} $(OH)_3$, and offer a provisional set of peak assignments based upon the highly variable M4- and A-site environments of the various T1 and T2 sites. Table 7 lists the Si-Na distances below 4.7 Å in crystal HMR-BO n. 1. There are two main groups of Si-Na interactions for both the Q^3 and Q^2 environments. Two Q^3 environments (T1A1 and T1B2) have three Na atoms closer than 4 Å; they should have the least-negative chemical shifts, and can be tentatively assigned to the peak at –88.7 ppm reported by Liu et al. (1996). The remaining

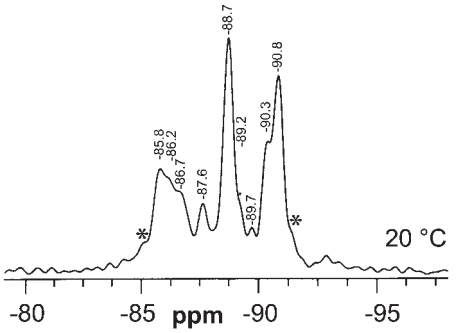

FIGURE 4. The room-T ^{29}Si CP MAS NMR spectrum of synthetic $NaNa_2Mg_5Si_8O_{21}(OH)_3$. Nine peaks are resolved and there are two possible additional peaks (*). Modified after Liu et al. (1996). Isotropic chemical shifts are relative to tetra-methyl-silane (TMS).

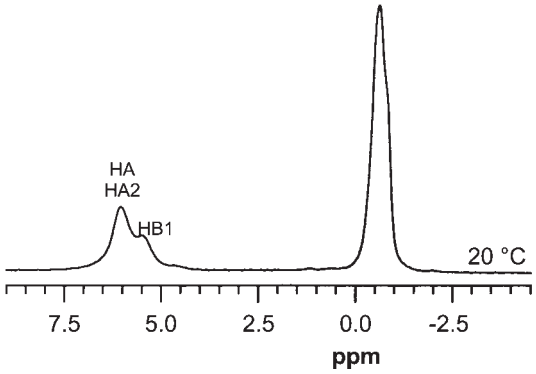

FIGURE 5. The room-T ^{1}H MAS NMR spectrum of synthetic $NaNa_2Mg_5Si_8O_{21}(OH)_3$ showing the peaks due to excess H at 5.5 and 6.1 ppm and the normal O3 protons at –0.6 ppm. The –0.6 ppm peak is a barely resolved doublet. Isotropic chemical shifts are relative to tetra-methyl-silane (TMS). The peaks are labeled according to the assignments discussed in the text. Modified after Liu et al. (1996).

TABLE 7. NNN environment of Si atoms in sample HMR-BO no.1

T1A1-	Na41	4.566	T1B2-	Na42	4.549	T1B-	Na4	4.650	T1A-	Na	4.268	T1A2-	Na1	4.443	T1B1-	Na1	4.511		
	Na1	3.880		Na1	3.934		Na	4.108		Na42	3.501		Na4	3.570		Na41	3.581		
	Na1	3.353		Na1	3.391		Na	3.245		Na	3.357		Na1	3.218		Na1	3.298		
	Na41	3.156		Na4	3.209		Na42	3.180											
T2A1-	Na1	3.581	T2B2-	Na4	3.744	T2B-	Na42	3.625	T2A-	Na42	4.321	T2A2-	Na4	4.198	T2B1-	Na41	4.376		
	Na41	3.574		Na1	3.642		Na	3.620		Na	3.844		Na42	3.820		Na1	3.933		
	Na41	3.245		Na42	3.203		Na4	3.373		Na4	3.555		Na1	3.805		Na41	3.737		
	Na41	3.047		Na4	3.079		Na42	2.973		Na42	3.166		Na4	3.062		Na41	3.110		

four Q^3 environments (T1A, T1B, T1A2, and T1B1) have two Na atoms at ~3.5–3.6 Å and ~3.2–3.35 Å, which implies more negative chemical shifts, and can be assigned to the peaks at –90.3 and –90.8 ppm reported by Liu et al. (1996). In particular, T1B is closest to the two Na atoms, and so may correspond to the –89.7 ppm peak. Also, two groups of Q^2 environments can be distinguished. The first group (T2B, T2A1, and T2B2) has four Na atoms in the interaction shell, and should be assigned to the less-negative chemical shifts, and thus to the broad peak at –85.8 ppm. The second group (T2A, T2A2, and T2B1) has three Na atoms in the interaction shell, implying more negative chemical shifts, and is assigned to the peaks at –86.2, –86.7, and –87.6 ppm.

The room-T ^{1}H MAS NMR spectrum of $NaNa_2Mg_5Si_8O_{21}(OH)_3$ (Liu et al. 1996; Fig. 5) has three peaks: one strong and sharp peak at –0.6 ppm, which was assigned to the two "standard" H pfu bonded to the O3 atoms, and two minor peaks at 5.5 and 6.1 ppm, which were assigned to excess H. The peak at 6.1 ppm has twice the area of the peak at 5.5 ppm, and the peaks merge and shift to 4.9 ppm at $T \geq 160$ °C. These isotropic chemical-shift values are typical of quite strongly hydrogen-bonded protons, and the progressive shift to 4.9 ppm with increasing T implies a weakening of hydrogen bonds (Berglund and Vaughan 1980; Brunet and Schaller 1996). Nevertheless, a value of 4.9 ppm indicates that we are still dealing with moderately strong hydrogen bonds. For example, the moderately strong interlayer hydrogen bonding in chlorite involves chemical shifts of around 4.3 ppm (Welch et al. 1995). These results can now be interpreted on the basis of the locations derived for excess H from crystal-structure details. The peak at 5.5 ppm should correspond to the HB1 position, which is located in a cavity with point symmetry $\bar{1}$ and thus represents one-third of an H pfu, whereas the peak at 6.1 ppm should correspond to HA and HA2, which represent two-thirds of an H pfu.

On close inspection, we see that the –0.6 ppm peak has two components, with a shoulder on the high-field side of the main peak, whereas the 240 °C spectrum of the $C2/m$ phase has only a single unsplit peak. The two-component nature of the –0.6 ppm peak is consistent with there being two different I-beam modules (*I* and *II*) in the room-temperature phase, both of which are adjacent to the HB1 proton.

The single-crystal structure determination reported here confirms that the synthetic amphibole of composition $NaNa_2Mg_5Si_8O_{21}(OH)_3$ is triclinic, space group $C\bar{1}$ with a tripling of the *b* edge, as indicated by electron diffraction. Furthermore, approximate positions for the excess protons have been identified. The proposed structure, including H positions, is strongly supported by all the available spectroscopic (NMR and IR) and chemical (EMPA, hydrogen extraction, and coulometric titration) studies of this amphibole. Thus, a unified picture of this extraordinary and elusive amphibole has now been achieved.

Acknowledgments

Useful comments by H. Yang and F.C. Hawthorne helped us to improve the clarity of the text.

References cited

Beran, A. and Libowitzky, E. (1999) IR spectroscopy and hydrogen bonding in minerals. In K. Wright and R. Catlow, Eds., Microscopic Properties and Processes in minerals, 493–508. Kluwer Academic Publishers.

Berglund, B. and Vaughan, R.W. (1980) Correlations between proton chemical shift tensors, deuterium quadrupole couplings, and bond distances for hydrogen bonds in solids. Journal of Chemical Physics, 73, 2037–2043.

Brese, N.S. and O'Keeffe, M. (1991) Bond-valence parameters for solids. Acta Crystallographica, B47, 192–197.

Brown, I.D. and Altermatt, U.D. (1985) Bond-valence parameters obtained from a systematic analysis of the inorganic crystal structure database. Acta Crystallographica, B41, 244–247.

Brunet, F. and Schaller, T. (1996) Protons in the magnesium phosphates phosphoellenbergerite and holtedahlite: An IR and NMR study. American Mineralogist, 81, 385–394.

Cameron, M. and Gibbs, G.V. (1971) Refinement of the crystal structure of two synthetic fluor-richterites. Carnegie Institution Washington Year Book, 70, 150–153.

Della Ventura, G. (1992) Recent developments in the synthesis and characterization of amphiboles. Synthesis and crystal-chemistry of richterites. Trends in Mineralogy, 1, 153–192.

Downs, R.T. and Hall-Wallace, M. (2003) The American Mineralogist Crystal Structure Database. American Mineralogist, 88, 247–250.

Gier, T.E., Cox, N.L., and Young, H.S. (1964) The hydrothermal synthesis of sodium amphiboles. Inorganic Chemistry, 3, 1001–1004.

Hamilton, D.L. and Henderson, C.M.B. (1968) The preparation of silicate compositions by a gelling method. Mineralogical Magazine, 36, 832–838.

Hawthorne, F.C. (1983) The crystal chemistry of amphiboles. Canadian Mineralogist, 21, 173–480.

Hawthorne, F.C., Della Ventura, G., Robert, J.L, Welch, M.D., Raudsepp, M., and Jenkins, D.M. (1997) A Rietveld and infrared study of synthetic amphiboles along the potassium-richterite-tremolite join. American Mineralogist, 82, 708–716.

Hawthorne, F.C., Oberti, R., Zanetti, A., and Czamanske, G.K. (1998) The role of Ti in hydrogen-deficient amphiboles: sodic-calcic and sodic amphiboles from Coyote Peak, California. Canadian Mineralogist, 36, 1253–1265.

Hawthorne, F.C., Oberti, R., Cannillo, E., Ottolini, L., Roelofsen, J., and Martin, R.M. (2001) Li-bearing arfvedsonitic amphiboles from the Strange Lake peralkaline granite, Quebec. Canadian Mineralogist, 39, 1161–1170.

Huggins, C.M. and Pimentel, G.C. (1956) Systematics of the infrared spectral properties of hydrogen bonding systems: frequency shift, half width and intensity. Journal of Physical Chemistry, 60, 1615–1619.

Iezzi, G., Della Ventura, G., Oberti, R., Cámara, F., and Holtz, F. (2004) Synthesis and crystal-chemistry of $Na(NaMg)Mg_5Si_8O_{22}(OH)_2$, a $P2_1/m$ amphibole. American Mineralogist, 89, 640–646.

Kemp, A.J. and Leake, B.E. (1975) Two hydrous-rich aluminous hornblendes. Mineralogical Magazine, 40, 308–311.

King, P.L., Hervig, R.L., Holloway, J.R., Vennemann, T.W., and Righter, K. (1999) Oxy-substitution and dehydrogenation in mantle derived amphibole megacrysts. Geochimica et Cosmochimica Acta, 63, 3635–3651.

Kuroda, Y., Hariya, Y., Suzuki, T., and Matsuo, S. (1975) Pressure effect on water content of amphiboles. Geophysical Research Letters, 2, 529–531.

Leake, B.E. (1968) A catalog of analyzed calciferous and sub-calciferous amphiboles together with their nomenclature and associated minerals. Geological Society of America, Special Paper 98, 210 pp. Boulder, Colorado.

Liu, S., Welch, M.D., Klinowski, J., and Maresch, W.V. (1996) A MAS NMR study of a monoclinic/triclinic phase transition in an amphibole with excess OH: $Na_3Mg_5Si_8O_{21}(OH)_3$ European Journal of Mineralogy, 8, 223–229.

Maresch, W.V. and Langer, K. (1976) Synthesis, lattice constants and OH-valence vibrations of an orthorhombic amphibole with excess OH in the system Li_2O-MgO-SiO_2-H_2O. Contributions to Mineralogy and Petrology, 56, 27–34.

Maresch, W.V., Miehe, G., Czank, M., Fuess, H., and Schreyer, W. (1991) Triclinic amphibole. European Journal of Mineralogy, 3, 899–903.

Nakamoto, K., Margoshes, M., and Rundle, R.E. (1955) Stretching frequencies as a function of distances in hydrogen bonds. Journal of American Chemical Society, 77, 6480–6486.

Novak, A. (1974) Hydrogen bonding in solids. Correlation of spectroscopic and crystallographic data. Structure Bonding, 18, 177–216.

Oberti, R., Ottolini, L., Della Ventura, G., and Prella, D. (2000) Excess OH in amphiboles: a structural model obtained by combining structure refinement, complete chemical characterization, and FTIR spectroscopy. Plinius, 24, 157.

Oberti, R., Cámara, F., Ottolini, L., and Caballero, J.M. (2003) Lithium in amphiboles: detection, quantification and incorporation mechanisms in the compositional space bridging sodic and ^{B}Li amphibole. European Journal of Mineralogy, 15, 309–319.

Phillips, R. (1963) The recalculation of amphibole analyses. Mineralogical Magazine, 33, 701–711.

Robert, J.L., Della Ventura, G., and Thauvin, J.-L. (1989) The infrared OH-stretching region of synthetic richterites in the system Na_2O-K_2O-CaO-MgO-SiO_2-H_2O-HF. European Journal of Mineralogy, 1, 203–211.

Rowbotham, G. and Farmer, V.C. (1973) The effect of "A" site occupancy upon the hydroxyl stretching frequency in clinoamphiboles. Contributions to Mineralogy

and Petrology, 38, 147–149.
Ruthmann, W. (1989) Synthese, Charakterisierung und Stabilitätsbeziehungen von Dreifachkettensilikaten im System Na_2O-MgO-SiO_2-H_2O. Unpublished Diploma Thesis, Ruhr-Universität Bochum, 86 p.
Semet, M.P. (1973) A crystal-chemical study of synthetic magnesiohastingsite. American Mineralogist, 58, 480–494.
Sheldrick, G.M. (1996) SADABS, Siemens area detector absorption correction software. University of Göttingen, Germany.
——— (1997a) SHELXTL-97—A program for crystal structure refinement. University of Göttingen, Germany. Release 97–2.
——— (1997b) SHELXS-97—A program for crystal structure solution. University of Göttingen, Germany. Release 97–2.
Vitek, E. and Maresch, W.V. (1985) Synthesis and stability relations of $Li_2Mg_2[Si_4O_{11}]$. European Journal of Mineralogy, 5, 1121–1131.
Welch, M.D. (1987) Experimental studies of selected amphiboles in the system Na_2O-CaO-MgO-Al_2O_3-SiO_2-H_2O-F_2 and its subsystems. Unpublished Ph.D. thesis, University of Edinburgh, 194 p.
Welch, M.D., Rocha, J., and Klinowski, J. (1992) Characterization of polysomatism in biopyriboles: Double-/triple-chain lamellar intergrowths. Physics and Chemistry of Minerals, 18, 460–468.
Welch, M.D., Barras, J., and Klinowski, J. (1995) A multinuclear NMR study of clinochlore. American Mineralogist, 80, 441–447.
Welch, M.D., Liu, S., and Klinowski, J. (1998) ^{29}Si MAS NMR systematics of calcic and sodic-calcic amphiboles. American Mineralogist, 83, 85–96.
Witte, P. (1975) Synthese und Stabilität von Amphibolphasen und wasserfreien Na-Mg-Silikaten im System Na_2O-MgO-SiO_2-H_2O, die Kompatibilitätsbeziehungen innerhalb des Si-reichen Teils des quaternären Systems oberhalb 600 °C im Druckbereich 1 atm–5kbar P(H_2O) und ihre petrologische Bedeutung. Unpublished Doctoral Dissertation, Ruhr-Universität Bochum, 256 p.
Witte, P., Langer, K., Seifert, F., and Schreyer, W. (1969) Synthetische Amphibole mit OH- Überschuß im System Na_2O-MgO-SiO_2-H_2O. Naturwissenschaften, 56, 414–415.
Zanetti, A., Vannucci, R., and Oberti, R. (1997) Crystal-(geo)chemical characterization of mantle amphiboles by SIMS, EMP and SREF analysis. Terra Nova, 9, 448.

MANUSCRIPT RECEIVED SEPTEMBER 25, 2003
MANUSCRIPT ACCEPTED JANUARY 29, 2004
MANUSCRIPT HANDLED BY MARC HIRSCHMANN